Neurotherapeutics (2021) 18:2073–2090
https://doi.org/10.1007/s13311-021-01090-x

ORIGINAL ARTICLE

Histone Mark Profiling in Pediatric Astrocytomas Reveals Prognostic Significance of H3K9 Trimethylation and Histone Methyltransferase SUV39H1

Alexia Klonou[1] · Penelope Korkolopoulou[2] · Antonios N. Gargalionis[1] · Dimitrios S. Kanakoglou[2] · Hector Katifelis[3] · Maria Gazouli[3] · Sarantis Chlamydas[1] · Andreas Mitsios[4] · Theodosis Kalamatianos[5] · George Stranjalis[5] · Marios S. Themistocleous[4] · Kostas A. Papavassiliou[1] · Spyros Sgouros[6] · Athanasios G. Papavassiliou[1] · Christina Piperi[1]

Accepted: 7 July 2021 / Published online: 7 July 2021

Abstract

Alterations in global histone methylation regulate gene expression and participate in cancer onset and progression. The profile of histone methylation marks in pediatric astrocytomas is currently understudied with limited data on their distribution among grades. The global expression patterns of repressive histone marks H3K9me3, H3K27me3, and H4K20me3 and active H3K4me3 and H3K36me3 along with their writers SUV39H1, SETDB1, EZH2, MLL2, and SETD2 were investigated in 46 pediatric astrocytomas and normal brain tissues. Associations between histone marks and modifying enzymes with clinicopathological characteristics and disease-specific survival were studied along with their functional impact in proliferation and migration of pediatric astrocytoma cell lines using selective inhibitors in vitro. Upregulation of histone methyltransferase gene expression and deregulation of histone code were detected in astrocytomas compared to normal brain tissues, with higher levels of SUV39H1, SETDB1, and SETD2 as well as H4K20me3 and H3K4me3 histone marks. Pilocytic astrocytomas exhibited lower MLL2 levels compared to diffusely infiltrating tumors indicating a differential pattern of epigenetic regulator expression between the two types of astrocytic neoplasms. Moreover, higher H3K9me3, H3K36me3, and SETDB1 expression was detected in grade III/IV compared to grade II astrocytomas. In univariate analysis, elevated H3K9me3 and MLL2 and diminished SUV39H1 expression adversely affected survival. Upon multivariate survival analysis, only SUV39H1 expression was revealed as an independent prognostic factor of adverse significance. Treatment of pediatric astrocytoma cell lines with SUV39H1 inhibitor reduced proliferation and cell migration. Our data implicate H3K9me3 and SUV39H1 in the pathobiology of pediatric astrocytomas, with SUV39H1 yielding prognostic information independent of other clinicopathologic variables.

Keywords Histone methylation · Pediatric astrocytomas · H3K9me3 · SUV39H1 · Survival

Introduction

Childhood brain tumors constitute the second most frequent type of solid tumors following hematologic malignancies, representing a main cause of mortality [1]. Pediatric astrocytomas are the most common brain neoplasms and encompass a heterogeneous group comprising the pilocytic astrocytomas (WHO grade I) which are relatively benign, circumscribed, slowly growing tumors, and the diffusely infiltrating astrocytomas of varying malignancy grades (WHO II to IV) which are characterized by a more aggressive behavior [2, 3]. Pilocytic astrocytomas only rarely progress to anaplastic tumors; they seldom recur

Athanasios G. Papavassiliou and Christina Piperi contributed equally to this work.

✉ Athanasios G. Papavassiliou
papavas@med.uoa.gr

✉ Christina Piperi
cpiperi@med.uoa.gr

Extended author information available on the last page of the article

and are largely amenable to surgical excision [2]. This group of tumors is characterized by several genetic alterations including activation of the RAS/MAP kinase pathway mostly (70%) resulting from a fusion of B-Raf proto-oncogene (BRAF) with KIAA1549, and the BRAFV600E mutation being identified in only 5% of pediatric cases [4]. On the other hand, 30% of high-grade diffusely infiltrating tumors harbor a missense mutation of histone H3 where lysine is replaced by methionine at position 27 (H3K27M) in the histone tail [5]. This recurrent mutation is a molecular hallmark of pediatric high-grade astrocytomas and demonstrates the fundamental role of histone code modifications in the development and progression of these tumors [5]. Another mutation of lower frequency, H3G34R/V, is also detected in pediatric astrocytomas, highlighting the important role of histone H3 integrity in the pathogenesis of high-grade diffusely infiltrating astrocytic tumors.

Post-translational modifications (PTMs) of histone tails constitute a major mechanism of epigenetic regulation of gene expression by affecting chromatin structure and forming binding sites for transcriptional regulators, such as DNA/histone-modifying enzymes, histone chaperones, chromatin remodelers, and transcription factors [6]. Histone PTMs participate in many cellular events, regulating DNA replication and repair, gene expression, chromatin compaction, and cell-cycle control [6]. Histone methylation of lysine residues depends on the recruitment of effector proteins and is mediated by specific enzymes—the histone lysine methyltransferases (HKMTs) [7]. Co-enrichment of active and repressive histone tail modifications may occur in gene promoters forming bivalent domains that can mediate a shift in gene expression from a poised state to active or inactive states in embryonic stem cells and cancer stem cells, thus promoting their plasticity and responsiveness [8].

Evidence has shown that trimethylation of histone H3 on lysine 9 (H3K9me3) and trimethylation of histone H3 on lysine 27 (H3K27me3) are associated with transcriptional silencing and heterochromatin structure [9]. H3K9me3 has been observed at repressed promoters and associates with chromosomal instability [10]. It often comingles and modulates the trimethylation of histone H4 on lysine 20 (H4K20me3) that is also involved in transcriptional silencing. Increased H3K9me3 expression has emerged as a prognostic factor in various cancers [11], and its levels are reportedly elevated in adult glioblastomas [12]. HKMTs catalyzing H3K9me3 include the SET domain family of proteins comprising SETDB1 and SUV39H1/2 which are often deregulated in human neoplasia, including adult astrocytic gliomas [12, 13]. Additionally, H3K27me3 is a hallmark of transcriptional repression and has been associated with tumorigenesis and metastasis [14, 15]. Overexpression of H3K27me3 methyltransferase EZH2 has been previously implicated in the pathogenesis of adult glioblastomas, lymphomas, and breast and prostate cancer [15–17].

On the other hand, active transcription is generally associated with trimethylation of histone H3 on lysine 4 (H3K4me3) and trimethylation of histone H3 on lysine 36 (H3K36me3) [18, 19]. H3K4me3 is an evolutionary conserved histone mark, enriched at the promoter region and transcription start sites of actively transcribing and poised genes [19]. An altered expression of H3K4me3 has been observed in adult glioblastomas and along with changes in H3K27me3 has been associated with regulation of transcription factors involved in repression of glioblastoma stem-like cell tumorigenicity [20]. Moreover, H3K4me3 has been proposed as a prognostic marker in hepatocellular and renal cell carcinoma [21]. H3K4me3 is mediated by MLL2/KMT2B in mammals, and its mutations highly increase cancer susceptibility. In concert, H3K36me3 regulates transcription initiation and elongation as well as DNA damage repair and RNA splicing [22]. Low levels of H3K36me3/H3K9me3 have been documented in glioma cells compared to normal astrocytes, and mutations of H3K36 writer SETD2 have been detected in adult gliomas [23, 24].

Based on the abovementioned studies, we hypothesized that changes in chromatin state may drive the development of pilocytic and diffusely infiltrating astrocytomas, characterized by differential expression of histone marks that regulate genes related to cancerous behavior, phenotypic plasticity, and patient outcome. In order to exploit our hypothesis, we have selected five histone lysine trimethylation marks H3K9me3, H3K27me3, H4K20me3, H3K4me3, and H3K36me3 that have been previously associated with tumorigenesis, but with limited data regarding their contribution to the pathobiology of pediatric astrocytomas.

The aim of this primary study was to investigate the global expression patterns of repressive H3K9me3, H3K27me3, and H4K20me3 and active H3K4me3 and H3K36me3 histone marks along with their respective modifying enzymes (SUV39H1, SETDB1, EZH2, MLL2, SETD2) in pediatric astrocytomas. We explored potential associations of histone marks and HKMTs with patients' clinicopathological features, degree of malignancy, and survival. Furthermore, we investigated the functional relevance of HKMTs in the proliferation and migration of pediatric astrocytoma cell lines CHLA-200 and SJ-GBM2 using selective inhibitors in vitro.

Materials and Methods

Patients and Tissue Sample Description

Our cohort consisted of 46 pediatric astrocytoma patients (1–15 years old) diagnosed at the Neurosurgery Department of 'Mitera' Children Hospital between 2017 and 2019. In all cases, the diagnosis and grading were peer-reviewed according to the principles laid down in the latest World Health Organization (WHO) Classification (2016) [2] and following the ethical standards as laid down in the 1964 Declaration of Helsinki and its later amendments or comparable ethical standards. All cases with available tumor tissue were included. Distinction between pilocytic astrocytomas (22 cases) and diffusely infiltrating astrocytomas (24 cases) glioblastomas was based on WHO criteria and genetic profiling of tumors (H3K27M, G34V/R, BRAFV600E, IDH1-R132H). The distribution per grade, the clinicopathological features, and genetic mutations are presented in Table 1. Written informed consent was obtained from the parents of all patients, and the study was approved by the University of Athens Medical School Ethics Committee (27/06/2017, 1,617,031,069). By the time this study was undertaken, 15 patients (32.6%) had died of disease after 24 (12–48) months whereas 26 patients (56.5%) were alive after 48 (24–60) months of follow-up. The remaining 5 patients (10.8%) had been lost from follow-up. Five (5) archival normal brain (cerebellum) tissues from children (1–3 years old) either frozen or in paraffin blocks were also used in the study.

Allele-Specific PCR Analysis

The detection of BRAF V600E mutation was performed by real-time allele-specific amplification as previously described [25]. Two forward primers were used with variations in their 30 nucleotides such that each was specific for the wild-type (V; AGGTGATTTTGGTCTAGCTAC AGT) or the mutated variant (E; AGGTGATTTTGGTCT AGCTACAGA), and one reverse primer (AS; TAGTAA CTCAGCAGCATCTCAGGGC). PCR genotyping results were confirmed by sequence analysis in representative samples. For the detection of G34V/R mutation, we performed allele-specific PCR as already described [26]. The primers used are shown below: G34GF: AGAGTGCGCCCTCTA CTGGAA (A allele), G34GF: AGAGTGCGCCCTCTACTG GAG (G allele), G34REV: AAGTCCTGAGCCATTTCT CGC (mutual primer), G34VF: GAGTGCGCCCTCTAC TGGAGT (V allele).

Table 1 Clinicopathological data of patients' cohort

Variable	Patients' cohort ($n = 46$) median (range)
Age	9 (2–15) years
	Number of cases (%)
Gender	
Male	28 (60.9)
Female	18 (39.1)
Grade	
I	22 (47.8)
II	7 (15.2)
III	2 (4.34)
IV	15 (32.6)
Tumor location	
Cerebellum	37 (80.4)
Brain stem	5 (10.9)
Temporal lobe	1 (2.2)
Occipital lobe	1 (2.2)
Frontal lobe	1 (2.2)
3rd ventricle	1 (2.2)
P53 expression (%)	36 (78.26)
H3K27M expression	11 (24)
BRAFV600E mutation	1 (2.2)
H3G34V mutation	2 (4.3)
IDH1 R132H expression	0
Surgery (total)	46 (100)
Partial resection	24 (52.2)
Complete resection	22 (47.8)
Radiotherapy	
Yes	15 (32.6)
No	31 (67.4)
Chemotherapy (TMZ)	
Yes	16 (34.7)
No	30 (65.2)

Reverse Transcription PCR Analysis and Semi-quantitative PCR

Total RNA was extracted from cultured pediatric astrocytic tissues using RNeasy Mini Kit (Qiagen, Hilden, Germany), according to the manufacturer's instructions. PrimeScript RT Reagent Kit-Perfect Real Time (Takara Bio, Japan) for RT-PCR was used for cDNA synthesis. For the semi-quantitative PCR, the produced cDNA was amplified with specific primer pairs for SETDB1, SUV39H1, EZH2, MLL2, and SETD2 genes (35 cycles) as well as

with GAPDH gene primer pairs (30 cycles) using KAPA 2G Multiplex Master Mix (KK5801, Sigma-Aldrich). The primer pairs were specifically designed using ENSEMBL and primer-BLAST and purchased from Eurofins Genomics (Table S1). PCR-amplified fragments were analyzed after their separation in agarose gels using image analysis software, ImageJ (La Jolla, CA, USA), and normalized to GAPDH levels.

Western Blot Analysis

Protein extraction from pediatric astrocytic cells and tissues was performed using ice-cold RIPA buffer (Thermo Fisher Scientific). Proteins were resolved by electrophoresis in SDS–polyacrylamide gels with several densities (6–15%) depending on the molecular weight of each protein. Subsequently, they were transferred to a nitrocellulose membrane (Porablot NCP, Macherey–Nagel, Germany). Membranes were blocked for 1 h at room temperature in Tris-buffered saline Tween-20 (TBS-T) with 5% nonfat milk and incubated with primary antibodies overnight at 4 °C. Dilutions of primary and secondary antibodies are presented in Table S2. After incubation with HRP-conjugated secondary antibodies, the detection of the immunoreactive bands was performed with the Clarity Western ECL Substrate (Bio-Rad). Relative protein amounts were evaluated by densitometry using ImageJ software (La Jolla, CA, USA) and normalized to the corresponding actin levels. All experiments have been performed at least 3 times and representative results are shown.

Immunohistochemical Staining

Immunostaining was performed on formalin-fixed paraffin-embedded sections (FFPE) sliced at 4-µm thickness as previously described [13] using the VECTASTAIN® Elite® ABC Universal Kit, PK-6200, Vector Laboratories). Details of primary antibodies are listed in Table S2. Paraffin sections from normal human breast tissue, breast cancer, colon cancer, hepatocellular cancer, and diffuse intrinsic pontine glioma (DIPG) tissues were used as positive controls, provided by the First Department of Pathology, Medical School, National and Kapodistrian University of Athens. Negative controls (i.e., sections in which the primary antibody was substituted with non-immune serum) were also stained in each run. Immunohistochemical evaluation was performed by a pathologist (PK) without knowledge of the clinical information. A Histoscore (*H*-score) based on the percentage of stained neoplastic cells (labeling index—LI) multiplied by staining intensity was calculated.

Cell Culture

The pediatric glioblastoma multiforme cell lines, CHLA-200 and SJ-GBM2, were kindly provided by the Texas Tech University Health Sciences Center, School of Medicine Cancer Center, COG Cell Line & Xenograft Repository (www.cccells.org). Cell lines were antibiotic-free, mycoplasma-free, authenticated, and validated by short tandem repeat (STR) genotyping. Cells were cultured in Iscove's Modified Dulbecco's Medium (IMDM, Biosera) supplemented with 1% penicillin–streptomycin (Gibco, Life Technologies), 20% fetal bovine serum (FBS) (Gibco, Life Technologies), 4 mM L-Glutamine (Gibco, Life Technologies), and 1 × ITS (Millipore, MA) (5 µg/mL insulin, 5 µg/mL transferrin, 5 ng/mL selenous acid). Cell cultures were incubated at 37 °C in a humidified atmosphere containing 5% CO_2–95% air.

Cell Viability Assay

The assessment of CHLA-200 and SJ-GBM2 cell viability was performed with the XTT Cell Proliferation Assay Kit (10,010,200, Cayman Chemical, USA). Cells were seeded in a 96-well plate at a density of 10^3–10^5 cells/well and treated with histone methylation inhibitors, BIX-01294 (382,190, Millipore, MA) at 100 µM, Mithramycin A (11,434, Cayman Chemical, USA) at 200 nM, UNC0638 (10,734, Cayman Chemical, USA) at 20 µM, DZNep (506,069, Millipore, MA) at 100 µM, and chaetocin (13,156, Cayman Chemical, USA) at 250 and 300 nM for 48 h. The following day, the medium was replaced with XTT diluted in serum-free, phenol red (PR)–free medium and mixed gently for 1 min on an orbital shaker. The cells were incubated for 2–4 h at 37 °C in a CO_2 incubator. The absorbance of each sample was measured using a microplate reader at 450 nm. Each experiment was conducted in triplicate.

Cell Migration Assay

CHLA-200 and SJ-GBM2 cells were cultured in 12-well culture wells at 4 sites (at a density of 10×10^5 cells per well). After the cells were coated, the cell monolayer was stained with a sterile 200-µL pipette tip (denoting zero migration), and media were added in the presence of chaetocin (250 nM, 300 nM). Following 24 h of incubation with the inhibitor, the samples were washed twice with PBS, pH 7.2. Each site was photographed on a computer-connected microscope at × 4 and × 20 magnifications. Phase-contrast images were taken at the start (0 h) and 24 h of incubation for the same region. Images were analyzed using WimScratch software (Wimasis image analysis platform). The results were expressed as percentages of the cell etched and covered area.

Data Mining

A series of bioinformatic analyses were conducted on a subset of a publicly available dataset of microarray (Affymetrix Human Genome U133 Plus 2.0 Array—Platform GPL570) pediatric brain samples (GSE50161), including 13 normal brain tissues and 49 glial tumors [27]. The differential gene expression pipeline was based on the workflow maEndToEnd (version 2.9.0) [28]. Another series of quality metrics were acquired by the Galaxy-based tool for interactive analysis of transcriptomic data (GIANT) [29]. All subsequent statistical analyses were performed with packages provided by the Bioconductor suite (version 3.12) [30] using the R language (version 4.0.3) (https://www.r-project.org/index.html) within RStudio (version 1.3.1093) (https://rstudio.com). The R2: Genomics analysis and visualization platform (http://r2.amc.nl) [31] was used to investigate the expression level of genes of interest in distinct glioma tissues.

Statistical Analysis

SPSS 25.0 software (SPSS Inc., Chicago, IL) and GraphPad Prism 6.0 were used for all graphical and statistical analyses, with a p-value < 0.05 considered statistically significant. Differences in the distribution of numerical variables among groups were tested with Student's t test, ANOVA, as appropriate. The immunohistochemical expression (H-score) of the enzymes and the histone marks was compared to the differential status of different parameters using the Mann–Whitney and Kruskal–Wallis tests as appropriate. Spearman's correlation test was employed in order to assess the correlation between the enzymes' and the histone marks' expression. Regarding the survival analysis, the survival time was calculated from the date of surgery until either the time of death or the 60 months of 5-year survival. Univariate survival analysis was conducted with the log-rank test, and cutoffs were determined according to the median H-score. In multivariate analysis, all parameters employed were treated as continuous variables using the Cox regression proportional hazards model. The statistical power of our study was calculated by conducting a multivariate general linear model having the type of tissue (normal or tumor) and grade of differentiation as fixed factors and the variable H-scores as dependent variables. The observed power is 0.95 ($p < 0.05$).

Results

Characterization of Patients' Tissue Samples

Based on histological analysis and genetic profiling of tumors (H3K27M, G34V/R, BRAFV600E, IDH1-R132H), twenty-two (22) cases (47.8%) were diagnosed as pilocytic astrocytomas and the remaining 24 cases (52.2%) as diffusely infiltrating astrocytoma grades II to IV. The distribution per grade, the clinicopathological features, and genetic mutations are presented in Table 1. Archival pediatric (1–3 years old) normal brain (cerebellum) tissues were used as controls.

Immunohistochemical Assessment of Repressive and Active Histone Marks in Normal Brain Tissues and Astrocytomas

The expression patterns of repressive and active histone PTMs in pediatric astrocytomas were investigated by immunohistochemistry in comparison to pediatric normal brain tissues. With regard to repressive marks expression, a significantly lower immunoreactivity of H4K20me3 was detected in normal brain tissues compared to grade I ($p = 0.005$) as well as to grade II–IV tumors ($p = 0.001$) (Kruskal–Wallis $p = 0.002$; Table 2; Figs. 1 and 2). Similar to H4K20me3, the active histone mark H3K4me3 expression was significantly lower in normal brain astrocytes compared to astrocytomas grade I ($p = 0.034$) and grades II–IV ($p = 0.036$) (Kruskal–Wallis $p = 0.028$). There were not statistically significant differences between normal brain

Table 2 Distribution (H-score) of repressive histone marks H3K9me3, H3K27me3, and H4K20me3, and active marks H3K4me3 and H3K36me3 in normal brain (NB) tissues and astrocytomas (grades I–IV)

	H3K9me3	H3K27me3	H4K20me3	H3K4me3	H3K36me3
	Mean (range)/no. of positive cases/total				
NB	126 (50–300)/5/5	150 (100–200)/5/5	50 (50–100)/4/5	56 (80–200)/2/5	210 (150–300)/5/5
Total	216 (45–300)/45/46	129 (2–300)/46/46	222 (10–300)/46/46	193 (30–300)/44/46	258 (45–300)/46/46
Grade I	199 (50–300)/22/22	142 (10–300)/22/22	212 (35–300)/22/22	190 (75–300)/22/22	272 (180–300)/22/22
Grade II	191 (45–285)/7/7	115 (2–200)/7/7	264 (180–300)/7/7	170 (50–300)/6/7	193 (45–300)/7/7
Grade III	300 (300)/2/2	120 (90–150)/2/2	300 (300)/2/2	245 (190–300)/2/2	300 (300)/2/2
Grade IV	241 (70–300)/14/15	119 (5–297)/15/15	207 (10–300)/15/15	200 (30–300)/14/15	261 (120–300)/15/15

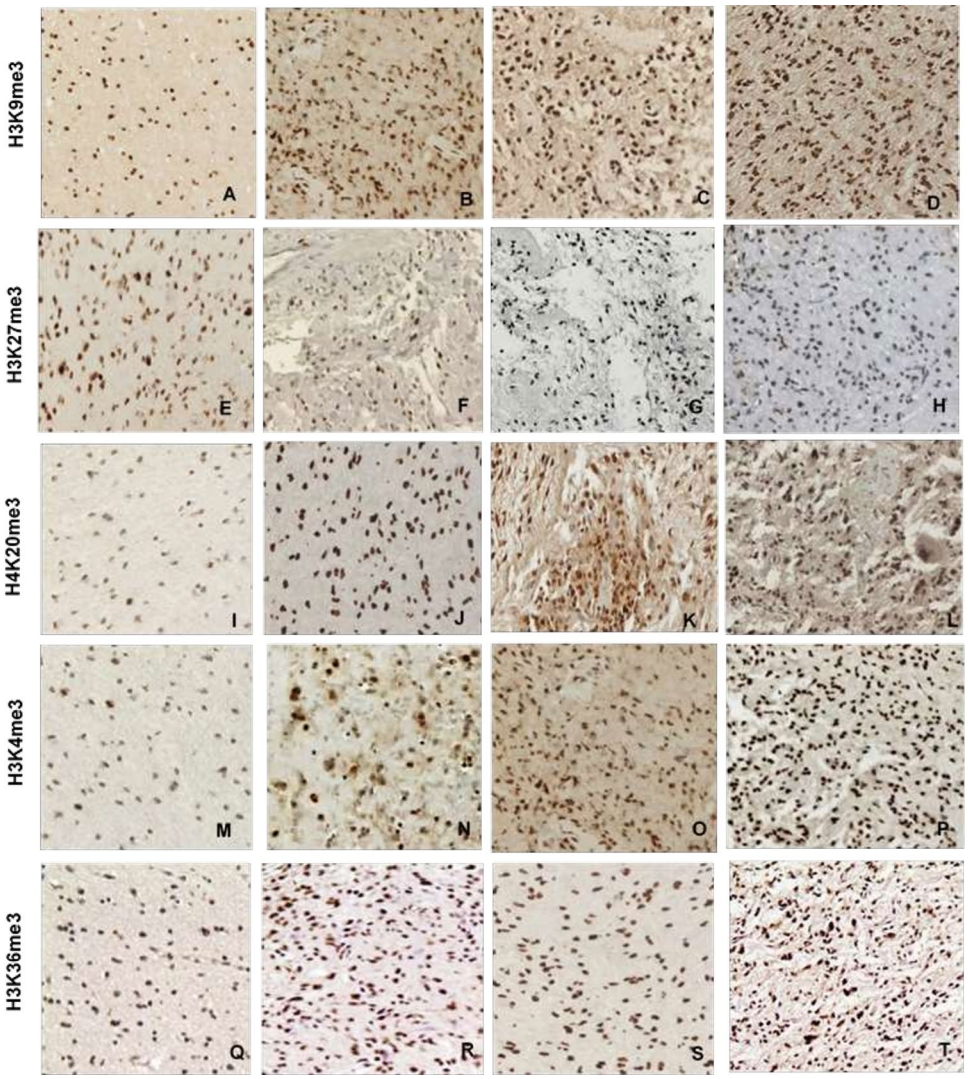

Fig. 1 Immunohistochemical expression of repressive histone marks H3K9me3, H3K27me3, and H4K20me3, and active marks H3K4me3 and H3K36me3 in normal brain tissues (**A**, **E**, **I**, **M**, **Q**), grade I (**B**, **F**, **J**, **N**, **R**), grade II (**C**, **G**, **K**, **O**, **S**), grade III (**D**, **H**, **P**), and grade IV (**F**, **T**) astrocytomas (magnification 20×)

and neoplastic tissues with regard to H3K9me3, H3K27me3, or H3K36me3 expression.

Differences in histone mark expression were further detected among astrocytomas of different histological grade. H3K9me3 immunoreactivity was observed in 45/46 (98%) of cases in the population cohort being significantly lower in grade II tumors compared to grade III–IV (Mann–Whitney *U* test $p=0.037$), although the overall association of H3K9me3 scores with grade attained only a marginal significance (Kruskal–Wallis $p=0.051$) (Figs. 1 and 2). H3K27me3 and H4K20me3 expression was observed in all cases (100%) without being significantly related to histological grade (Fig. 1). With respect to active marks, nuclear H3K4me3 staining was observed in 44/46 neoplastic cases with no significant difference being observed among grade I, II, and III–IV cases (Fig. 1). H3K36me3 immunoreactivity was observed in all cases (100%) and was significantly associated with astrocytoma grade (Kruskal–Wallis $p=0.031$), being lower in grade II as compared to both grade I ($p=0.029$) and III–IV cases ($p=0.05$; Figs. 1 and 2).

Correlation analysis revealed that the H3K9me3 *H*-score was higher in grade IV tumors bearing H3K27M mutation (Mann–Whitney U test, $p=0.033$; Fig. 2). A positive correlation was observed between the H3K9me3 *H*-score on the one hand and the active marks H3K4me3 *H*-score (Spearman's correlation, $R=0.603$, $p<0.001$) or H3K36me3 *H*-score (Spearman's correlation, $R=0.307$, $p=0.038$), on the other.

mRNA Analysis of Histone Lysine Methyltransferases in Pediatric Astrocytomas Compared to Normal Brain Tissues

Following the differences in histone marks between normal brain tissues and astrocytomas, we proceeded with evaluation of the respective histone lysine methyltranferase gene expression. Bioinformatic analysis of a publicly

available microarray dataset of pediatric astrocytoma samples (GSE50161), comprising 13 normal brain tissues and 49 glial tumors (15 pilocytic astrocytomas and 34 glioblastomas) [31], using the R2: Genomic Analysis and Visualization platform (http://r2.amc.nl) [36] revealed that pediatric astrocytomas showed a significant increase of SUV39H1, SETDB1, EZH2, MLL2, and SETD2 gene expression compared to normal brain tissues (Fig. 3A). In order to confirm these data in our cohort, we evaluated the mRNA levels of these HKMTs in normal brain tissue samples and astrocytomas by qRT-PCR. In concert with in bioinformatic data, we detected an upregulation of SUV39H1, SETDB1, EZH2, MLL2, and SETD2 mRNA levels in pediatric astrocytomas compared to normal brain tissues without major differences among grades after normalization with the GAPDH housekeeping gene (Fig. 3B, C).

Immunohistochemical Assessment of Histone Lysine Methyltransferases in Normal Brain Tissues and Pediatric Astrocytomas and Correlation with Clinicopathological Characteristics

To further investigate protein expression of HKMTs in normal brain tissues and pediatric astrocytomas, we proceeded with immunohistochemical analysis. Normal brain astrocytes did not express SUV39H1, EZH2, and SETD2. The nuclear expression of SETDB1 that catalyzes the H3K9me3 mark was significantly lower in normal brain tissues compared to grade I ($p=0.014$) and grade II–IV astrocytomas ($p=0.008$) (Kruskal–Wallis $p=0.008$; Table 3). Accordingly, SUV39H1 expression was significantly elevated in grade I tumors ($p=0.008$), although no difference could be seen between normal brain tissue and grades II–IV (Kruskal–Wallis $p=0.01$). Nuclear EZH2 immunoreactivity was absent in normal brain tissues and expressed in very low levels in astrocytomas (H-score = 0.5–12.5), the difference being statistically non-significant (Fig. 4). Neoplastic tissues exhibited increased SETD2 levels, in terms of both grade I ($p=0.014$) and grades II–IV ($p=0.008$) (comparisons with regard to normal brain, Kruskal–Wallis $p<0.001$). The immunoreactivity of MLL2 that mediates the H3K4me3 mark did not significantly differ among normal and neoplastic brain tissues.

We proceeded with investigation of HKMT expression among astrocytomas of different grade. Nuclear expression of SETDB1 was observed in 43/46 cases (93.5%). SETDB1 expression was significantly lower in grade II compared to grade III–IV tumors ($p=0.046$). SETDB1 H-score was positively correlated with H3K9me3 expression ($R=0.344$, $p=0.019$).

On the contrary, the histone methyltransferase EZH2 that mediates H3K27me3 mark was expressed in very low levels in 10/46 (21.7%) pediatric astrocytomas of all grades without any association with grade. MLL2 immunoreactivity was observed in 28/46 (60.8%) cases being significantly lower in grade I compared to grade III–IV tumors ($p=0.032$), but no statistical significance was reached between grade II and grade III–IV tissues (Kruskal–Wallis $p=0.029$; Fig. 4). MLL2 H-score was positively correlated with p53 expression ($R=0.335$, $p=0.023$). Moreover, SETD2 immunostaining was detected in all astrocytoma cases without being associated with grade (Table 3).

Western Blot Analysis of HKMT and Histone Marks Protein Levels in Normal Brain Tissues and Pediatric Astrocytomas

In order to quantitate the protein levels of HKMTs in normal brain tissues and astrocytomas, we performed western blot analysis. SETDB1 and SUV39H1 protein levels were markedly lower in normal brain compared to astrocytomas. Among tumors, SETDB1 levels were increased with grade, being higher in grade IV samples. SUV39H1 levels were higher in grade I astrocytomas compared to grade IV tumors. Very low protein levels of EZH2 protein were detected in grade I and II astrocytomas and none in normal brain tissues. On the other hand, MLL2 protein levels were higher in astrocytomas II and IV compared to normal brain and grade I tumors. SETD2 levels were not detected in normal brain and were higher in grade IV astrocytomas compared to grades I and II (Fig. 5A). All the abovementioned data were in broad agreement with the immunohistochemical expression of HKMTs in normal brain tissues and astrocytomas.

Following detection of HKMT protein levels, we proceeded with evaluation of histone marks in astrocytomas and normal brain tissues by western blot (Fig. 5B). H3K9me3 protein levels were detected in normal brain tissues and in astrocytomas being higher in astrocytic tumors irrespective of grade. H4K20me3 and H3K4me3 protein levels were detected only in astrocytomas and not in normal brain, without exhibiting any difference among tumors. H3K27me3 and H3K36me3 protein levels were detected in normal brain and astrocytomas, without difference among tumor grades. The protein levels of all histone marks in normal brain tissues and astrocytomas were in broad agreement with the immunohistochemical data described above.

Survival Analysis

Univariate survival analysis was carried out in the entire cohort of pediatric astrocytomas, and the results are presented in Table 4. Among all examined parameters, those associated with reduced patient survival included high grade (III/IV) ($p<0.001$), partial surgical tumor excision ($p<0.001$), absence of radiotherapy ($p=0.026$), high Ki-67 expression ($p=0.021$), the presence of H3K27M

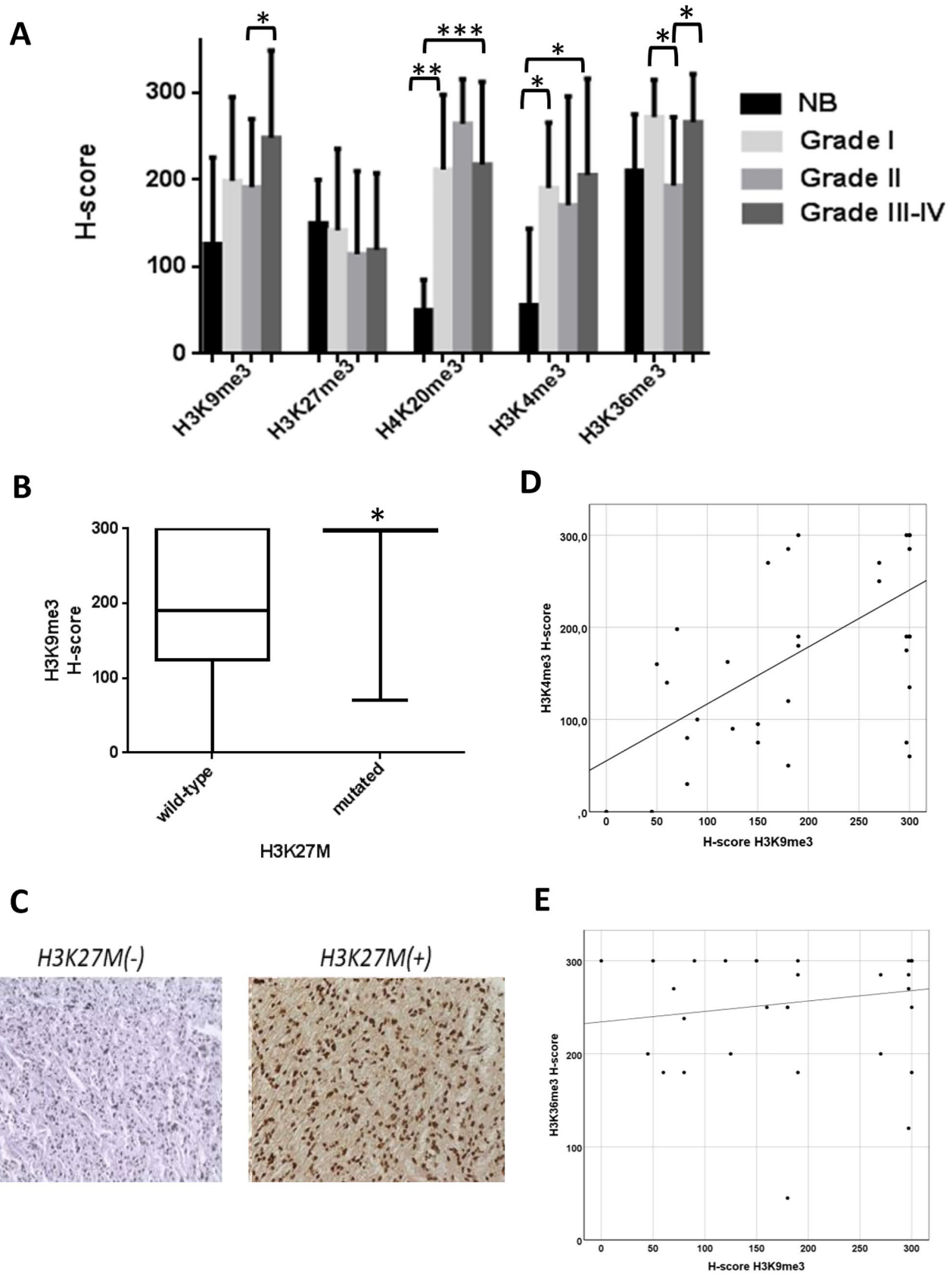
A
H-score
300
200
100
0
NB
Grade I
Grade II
Grade III-IV
H3K9me3
H3K27me3
H4K20me3
H3K4me3
H3K36me3
B
H3K9me3 H-score
wild-type
mutated
H3K27M
C
H3K27M(-)
H3K27M(+)
D
H3K4me3 H-score
H-score H3K9me3
E
H3K36me3 H-score
H-score H3K9me3

◂**Fig. 2** **A** Histone mark expression (H-score) in normal brain tissues and astrocytomas according to histological grade. **B**, **C** H3K9me3 expression (*H*-score) was increased in astrocytoma grade IV bearing H3K27M mutation ($p=0.033$). **D** H3K9me3 H-score was positively correlated with H3K4me3 *H*-score ($p<0.001$, correlation coefficient = 0.603) and **E** with H3K36me3 *H*-score ($p=0.038$, correlation coefficient = 0.307). *$p<0.05$, **$p<0.01$, ***$p<0.001$

mutant protein ($p<0.001$; Fig. 6A), increased H3K9me3 expression ($p=0.05$; Fig. 6B), decreased SUV39H1 expression ($p=0.022$; Fig. 6C), and increased MLL2 expression ($p=0.048$; Fig. 6D). Stratified univariate analyses separately for pilocytic and diffusely infiltrating tumors revealed that grade III/IV tumors were associated with reduced survival compared to grade II tumors ($p=0.028$). Furthermore, elevated H3K9me3 and H3K4me3 expression was associated with reduced patient survival among diffusely infiltrating tumors ($p=0.03$ and $p=0.021$, respectively; Table 4).

Multivariate survival analysis results, including the above parameters which turned out to be significant in univariate analysis, selected only SUV39H1 expression (HR = 0.218 $p=0.050$) along with histological grade (HR = 13.78 $p=0.002$) as independent predictions of patients' survival.

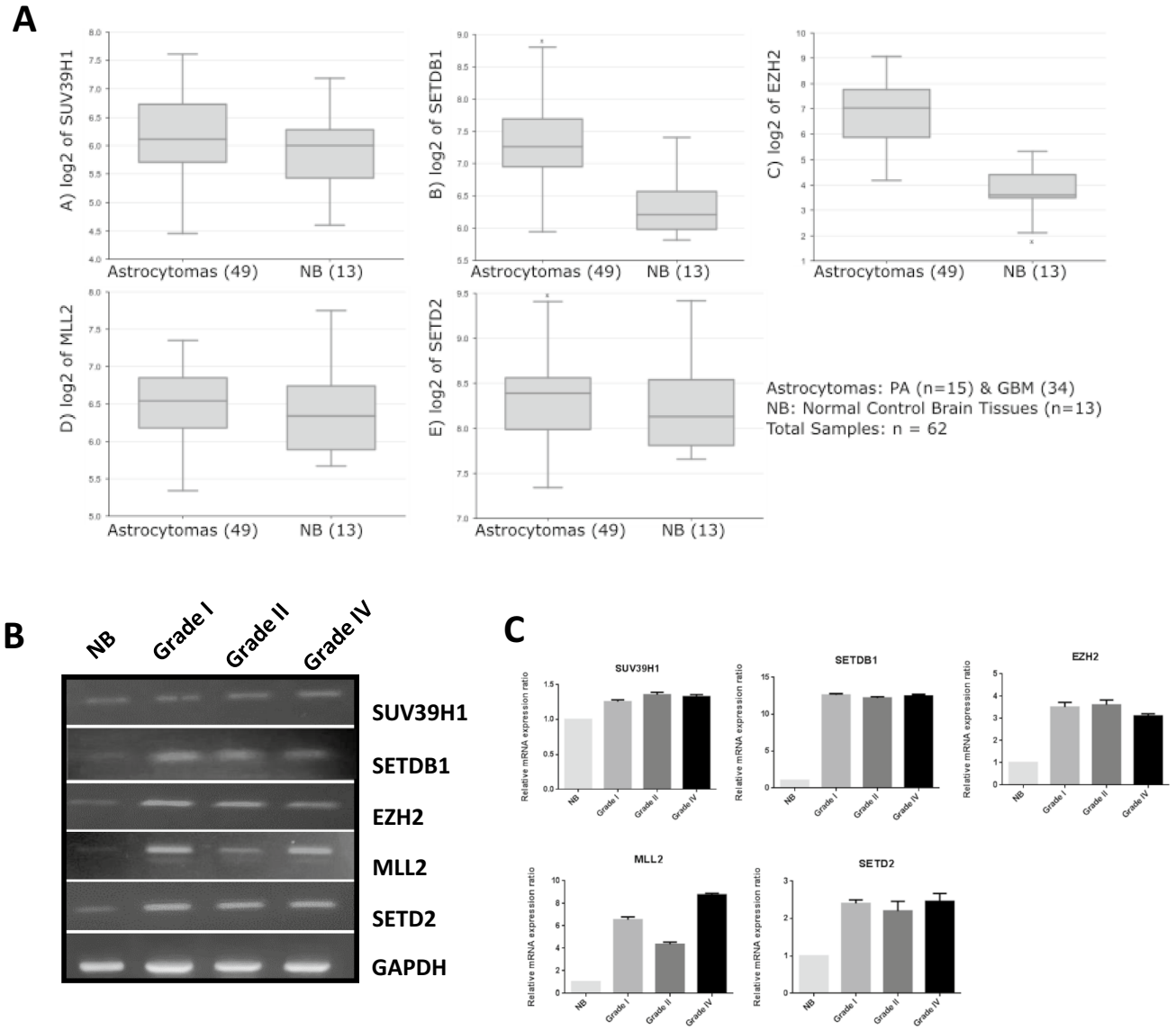

Fig. 3 Bioinformatic analysis of HKMTs in pediatric astrocytomas. **A** Box plot comparisons of SUV39H1 ($p=0.130$), SETDB1 ($p=1.49\times10^{-6}$, EZH2 ($p=8.44\times10^{-11}$, MLL2 ($p=0.476$), SETD2 ($p=0.445$). The GSE50161 subsets were analyzed by one-way analysis of variance (ANOVA) through the R2: Genomics analysis and visualization platform. **B**, **C** Detection of HKMT mRNA levels in normal brain tissues and astrocytomas by qRT-PCR

Impact of HKMT Inhibition in Cell Viability of Pediatric Astrocytoma Cell Lines

Following the emerging prognostic significance of elevated H3K9me3 and SUV39H1 in astrocytomas, we proceeded to investigate the functional role of histone lysine trimethylation in pediatric grade IV astrocytoma cell lines CHLA-200 and SJ-GBM2. We used several commercially available HKMT inhibitors such as BIX-01294 and UNC0638 (GLP and G9a inhibitors), chaetocin (SUV39H1 inhibitor), DZNep (EZH2 inhibitor), and Mithramycin A (DNA methyltransferase inhibitor). CHLA-200 and SJ-GBM2 cell viability was significantly decreased after treatment with chaetocin by 64.8% and 47.4%, respectively ($p < 0.001$) (Fig. 7A, B). The cell viability of CHLA-200 and SJ-GBM2 cells was reduced by 22% and 14.5% after BIX-01294 treatment and by 31.4% and 9.9% upon UNC0638 treatment. The DNA methylation inhibitor, Mithramycin A, reduced cell viability by 9% and 23.3% respectively compared to control (Fig. 7A, B). No effect on cell viability was observed upon treatment with the inhibitor DZNep compared to control.

Impact of SUV39H1 Inhibitor Chaetocin in Cell Viability and Migration of Pediatric Astrocytoma Cell Lines

To further investigate the functional significance of SUV39H1 in pediatric astrocytomas, we treated pediatric astrocytoma cell lines CHLA-200 and SJ-GBM2 cells with the chemical inhibitor chaetocin at different concentrations (250 nM and 300 nM) for 48 h (Fig. 7C). After 48 h treatment, we verified inhibition of SUV39H1 protein levels by western blot analysis. Reduced expression of SUV39H1 was detected at 250 nM and at 300 nM of chaetocin. For the assessment of glioma cell proliferation after SUV39H1 inhibition, XTT assay was performed at 48 h of culture. Upon chaetocin treatment, CHLA-200 and SJ-GBM2 cell viability was significantly decreased compared to mock cells ($p < 0.001$ at both time points, respectively). Specifically, the CHLA-200 cell viability was reduced to 66.3% at 250 nM chaetocin and 64.3% at 300 nM chaetocin treatment while SJ-GBM2 cell viability was decreased to 47.5% and 45.6%, respectively (Fig. 7D).

We proceeded to investigate the effects of SUV39H1 inhibition on astrocytoma cell migration; monolayer scratch migration assays were performed 24 h after 250 nM and 300 nM chaetocin treatment (Fig. 7E). Cell migration in the scratch area was reduced by 25.7% and 12.1% in CHLA-200 and by 11.2% and 16.5% in SJ-GBM2 chaetocin-treated cells, respectively (Fig. 7E). Wound recovery in CHLA-200 was 100% in untreated control, 69.6% and 51.4% in 250 nM and 300 nM chaetocin-treated cells respectively ($p < 0.001$). In SJ-GBM2, the wound recovery was 93.2% in mock, and 77.7% and 72.7% after treatment with 250 nM and 300 nM chaetocin, respectively ($p < 0.001$) (Fig. 7F). These data indicate the suppressive effect of SUV39H1 inhibition in the migratory capacity of glioma cells.

Discussion

Genome-wide studies have revealed that the organization of chromatin structure relies on histone modifications to functionally regulate transcription factor binding. In several cancer types, multiple methyl marks have been shown to change in concert, highlighting the importance of combinatorial modification effect on biological function [11, 13, 20, 21]. In the present study, we hypothesized that different histone marks characterize pilocytic and diffuse infiltrating astrocytomas that may regulate genes related to malignancy, phenotypic plasticity, and patients' outcome.

The expression patterns of three repressive histone methylation marks (H3K9me3, H4K20me3, H3K27me3) and two

Table 3 Distribution (H-score) of SETDB1, SUV39H1, EZH2, MLL2, and SETD2 in normal brain tissues and astrocytomas (grades I–IV)

	SETDB1	SUV39H1	EZH2	MLL2	SETD2
	Mean (range)/no. of positive cases/total				
NB	15 (25–50)/ 2/5	0	0	32 (10–70)/ 4/5	0
Total	128 (10–285)/ 43/46	96 (2–300)/ 31/46	1.4(0.5–12.5)/ 10/46	66 (3–270)/ 28/46	173 (10–300)/ 46/46
Grade I	116 (20–270)/ 20/22	112 (25–300)/ 16/22	1.9 (0.5–12.5)/ 6/22	25 (4–160)/ 10/22	183 (10–300)/ 22/22
Grade II	77 (10–255)/ 7/7	101 (10–270)/ 5/7	1.4 (10)/ 1/7	112 (3–240)/ 6/7	149 (70–297)/ 7/7
Grade III	170 (70–270)/ 2/2	15 (30)/ 1/2	6 (2–10)/ 2/2	60 (120)/ 1/2	110 (30–190)/ 2/2
Grade IV	165 (30–285)/ 14/15	65 (2–270)/ 9/15	0.2 (3)/ 1/15	105 (15–270)/ 11/15	177 (40–300)/ 15/15

active (H3K4me3, H3K36me3) were investigated along with their modifying enzymes and assessed their potential usefulness as diagnostic and prognostic biomarkers in pediatric astrocytomas. By using bioinformatic analysis of public databases, we have detected a significant upregulation of the respective histone methyltransferases in pediatric astrocytomas compared to normal brain tissues that was further confirmed by mRNA quantitation, indicating a possible deregulation of histone methylation marks distribution.

All three repressive marks were detected in astrocytomas with higher H3K9me3, H4K20me3, and lower H3K27me3 levels than in normal brain tissues. The lower expression of the H3K27me3 mark in astrocytomas is in accordance with a previous investigation where reduced H3K27me3 levels in high-grade pediatric tumors were most possibly attributed to the presence of H3K27M mutation [32]. This mutation causes Lys27Met (K27M) substitution at a critical regulatory location on the N-terminal tail of H3, affecting

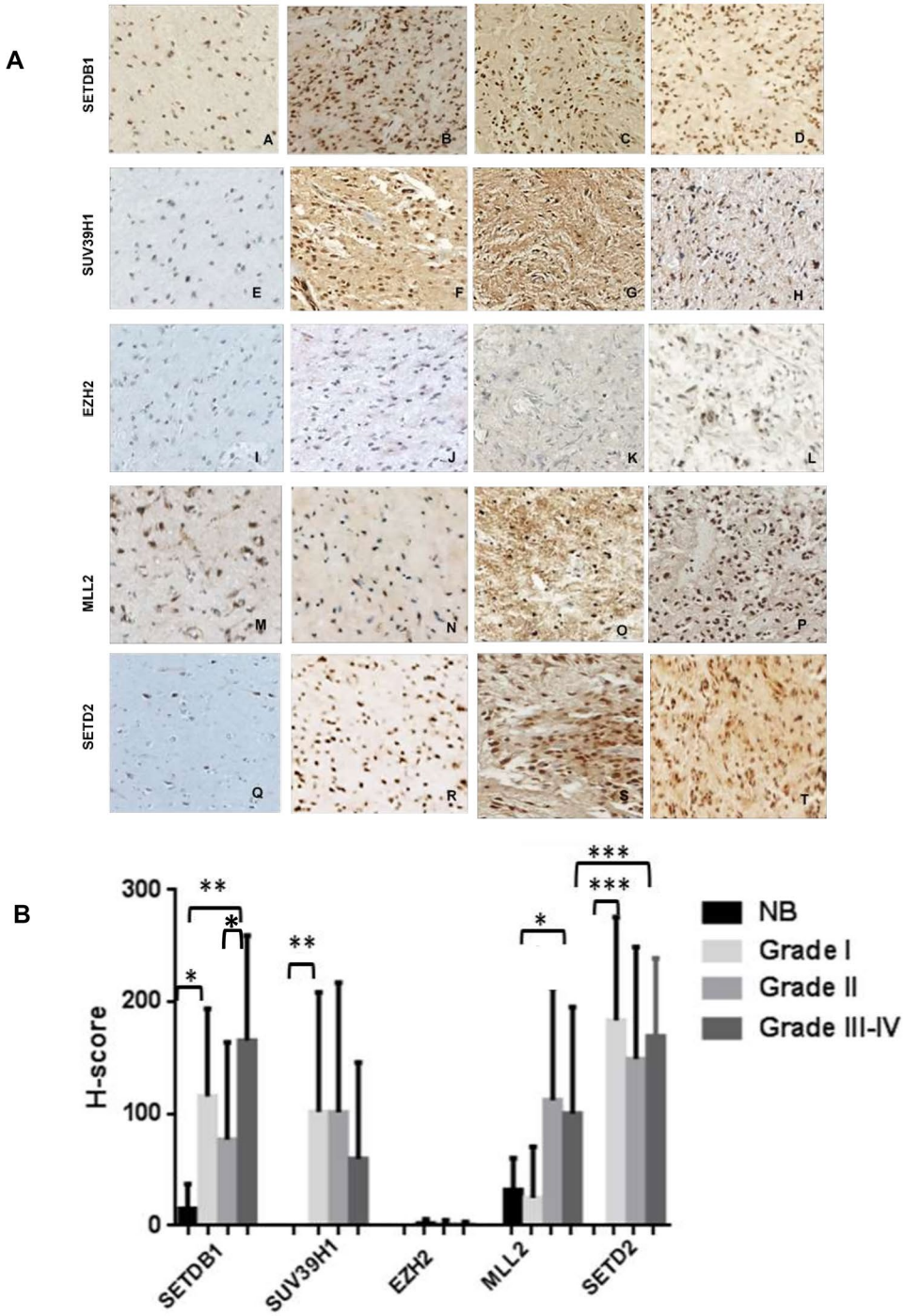

Fig. 4 **A** Immunohistochemical expression of SETDB1, SUV39H1, EZH2, MLL2, and SETD2 in normal brain tissues (A, E, I, M, Q), grade I (B, F, J, N, R), grade III (D, H, T), and grade IV (L, P) astrocytomas. **B** Distribution of HKMT expression in normal astrocytes and astrocytomas of different grade. $*p<0.05$, $**p<0.01$, $***p<0.001$

chromatin structure and regulation of gene transcription [32, 33]. H3K27M mutation further associates with H3K27me3 loss and H3K27Ac gain in distinct genomic regions. In our cohort, decreased H3K27me3 staining was also detected in H3K27M mutant tumors compared to wild type (36% vs. 49%, respectively), in accordance with previous studies [32, 33]. Furthermore, the oncohistone H3K27M has been shown to inhibit the polycomb repressive complex 2 (PRC2), a multiprotein complex responsible for H3K27me3 by binding to the catalytic subunit EZH2 and preventing its automethylation. In this way, it blocks EZH2 methyltransferase activity that is required for attaining proper cellular levels of H3K27me3 [34]. In accordance, H3K27M presence may account for the reduced protein expression levels of EZH2 detected in our cohort, as previously observed [35–37].

In regard to the upregulation of the repressive H3K9me3 mark, there are only very few data available on its abundance in pediatric astrocytomas [35, 38]. Our immunohistochemical analysis revealed high levels of H3K9me3 expression in all groups of pediatric astrocytomas. Increased immunoreactivity of H3K9me3 was observed in grade III/IV compared to grade II tumors and was further validated by western blot analysis. A study investigating loss of histone marks, has detected a low frequency of H3K9me3 loss (18%) in pediatric GBM [35] while similar H3K9me3 expression levels have been reported in diffuse intrinsic pontine glioma (DIPG) and extrapontine adult and pediatric GBM [38]. In our cohort, the rate of H3K9me3 loss in grade IV tumors was 6%. We have previously detected lower H3K9me3 levels in adult astroglial tumors, especially of higher grades, compared to adjacent normal brain tissues [13], indicating that this histone mark is differentially regulated in the context of pediatric and adult gliomagenesis. In adult tumors, low H3K9me3 levels are most likely attributed to global DNA hypomethylation prevailing in high-grade gliomas as opposed to normal brain tissues [13] and possibly

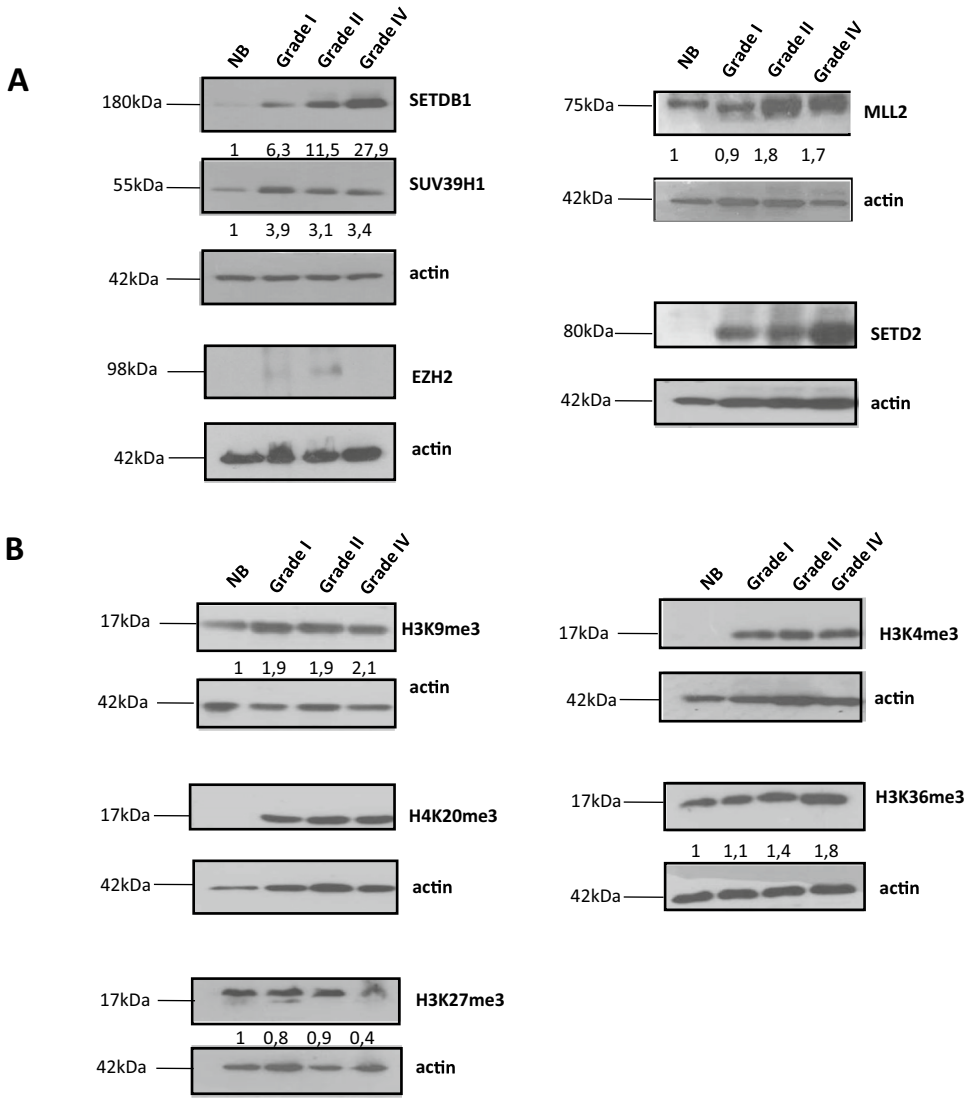

Fig. 5 Detection of **A** HKMTs and **B** histone marks protein levels by western blot in normal brain tissues and astrocytomas. All experiments were repeated at least three times, and representative data are shown. Densitometric quantification of protein levels was performed based on normalization to actin levels

associate with IDH1 mutation [39]. Furthermore, H3K9me3 levels were positively correlated in our cohort with the presence of H3K27M mutation, indicating that this histone mark may represent the driving force behind K27M mutation in astrocytomas. This is in accordance with recent data reporting H3K9me3 detection in 75% of K27M mutant pediatric GBM cases [35] suggesting that poor survival of H3K27M patients may be driven by alterations of H3K9me3 and needs further validation.

A major finding of our study is the prognostic effect of H3K9me3 expression in the entire cohort where high H3K9me3 levels were correlated with reduced patients' survival. Moreover, in the stratified Cox proportional-hazard model of the two tumor types separately, univariate analysis showed that high H3K9me3 levels were significantly associated with reduced patients' survival in diffusely infiltrating astrocytomas. Given the repressive role of this histone mark to gene expression and its correlation with the presence of H3K27M mutant protein, our results indicate that elevated H3K9me3 expression might underlie biologic aggressiveness in pediatric astrocytomas, possibly by inhibiting the expression of tumor suppressor genes.

Furthermore, H3K9me3 often comingles with the repressive mark H4K20me3 which regulates the expression of genes that control mesenchymal–epithelial transition and is involved in telomere length maintenance [9, 11, 13]. In our study, significantly high levels of H4K20me3 were detected in pediatric astrocytomas, both pilocytic and diffusely infiltrating ones compared to normal brain tissues, suggesting the significant involvement of H4K20me3 in pediatric glial tumorigenesis as observed in other tumor types [11, 13].

Our data also reveal a positive correlation of H3K9me3 expression with the H3K4me3 levels indicating a possible synergistic action in gene regulation in astrocytomas. H3K4me3 domains have been found enriched at transcription start sites (TSS), increasing enhancer activity and defining active tumor suppressor genes [18, 19]. We detected increased immunoreactivity of H3K4me3 in pilocytic and diffusely infiltrating tumors compared to normal brain but without any statistically significant association with grade. This finding argues in favor of the involvement of this particular histone modification in the early stages of pediatric glial tumorigenesis. In agreement, a previous study on pediatric GBM has demonstrated homogeneous nuclear localization of H3K9me3 and H3K4me3 marks as well as increased H3K4me3 staining and altered histone code along with G34V/R mutation [40]. Additionally, increased H3K4me3 levels were shown to regulate several cancer-associated genes in H3K27M-mutant high-grade pediatric gliomas [41]. Recently, a bivalent histone methylation signature, H3K4me3-H3K9me3, has been reported to regulate the expression of rDNA genes, zinc finger protein, long non-coding RNAs, and developmental signal proteins with tumor promoting functions [42]. Furthermore, the H3K9 HKTMs, SETDB1 and SUV39H1, demonstrated sensitivity

Table 4 Results of univariate survival analysis (long-rank test) for overall survival

	Entire cohort (p)/hazard ratio 95% CI	Pilocytic astrocytomas (p)/hazard ratio 95% CI	Diffusely infiltrating astrocytomas (p)/hazard ratio 95% CI
Histological grade (I vs II vs III/IV)	**< 0.001**/8.1 [2.5, 27.1]	-	**0.028**/3.8 [0.8–17.8]
Age (< 8.4 vs ≥ 8.5)	0.479/0.7 [0.2, 2.0]	0.812/1.01 [0.1–7.5]	0.949/0.97 [0.3–2.8]
Gender (1: male, 2: female)	0.389/1.6 [0.5, 4.6]	0.071/1.3 [0.2, 7.1]	0.371/1.5 [0.5–4.5]
Surgical excision (complete/partial)	**< 0.001**/106.7 [1.4, 7990.8]	–	0.393/1.3 [0.7–2.7]
Chemotherapy (+/−)	0.526/1.4 [0.5, 4.1]	0.75/ 0.7 [0.08–6.1]	0.969/0.9 [0.3–2.8]
Radiation (+/−)	**0.026**/3.2 [1.0, 10.5]	0.661/0.3 [0.002–49.6]	**0.029**/3.3 [0.9–11.6]
Ki-67 expression (%) (< 3 vs ≥ 3)	**0.021**/6.9 [0.9, 53.2]	0.077/0.3 [0.02–2.8]	0.723/1.3 [0.2–10.4]
p53 expression (%) (< 5 vs ≥ 5)	0.057/3.6 [0.8, 16.4]	**0.003/33.3 [2.7–410.6]**	0.993/0.9 [0.2–4.4]
H3K27M expression (positive vs negative)	**< 0.001**/0.15 [0.05, 0.43]	–	0.107/2.1 [0.7–6.2]
H3K9me3 H-score (< 270 vs ≥ 270)	**0.05**/2.7 [0.9, 8.5]	0.077/0.3 [0.02–5.7]	**0.03**/2.8 [0.9–9.1]
H3K27me3 H-score (< 100 vs ≥ 100)	0.267/0.6 [0.2, 1.6]	0.057/0.3 [0.05–2.4]	0.947/1.03 [0.4–2.9]
H4K20me3 H-score (< 250 vs ≥ 250)	0.536/1.4 [0.5, 3.9]	0.465/1.1 [0.03–42.4]	0.44/0.7 [0.2–2.0]
H3K4me3 H-score (< 190 vs ≥ 190)	0.136/2.2 [0.7, 7.0]	0.061/2.1 [0.2–20.2]	**0.021**/3.0 [0.9–9.5]
H3K36me3 H-score (< 300 vs ≥ 300)	0.991/0.9 [0.4, 2.8]	0.537/3.4 [0.4–29.4]	0.404/1.4 [0.5–3.9]
SETDB1 H-score (< 120 vs ≥ 120)	0.644/1.2 [0.4, 3.4]	0.858/7.1 [0.8–60.3]	0.32/1.5 [0.6–4.4]
SUV39H1 H-score (< 30 vs ≥ 30)	**0.022**/0.3 [0.1, 0.9]	0.493/0.3 [0.05–1.9]	0.089/0.5 [0.2–1.3]
EZH2 H-score (< 0.5 vs ≥ 0.5)	0.243/0.5 [0.1, 1.8]	0.091/0.2 [0.02–2.3]	0.253/0.5 [0.2–1.9]
MLL2 H-score (< 15 vs ≥ 15)	**0.048**/2.8 [0.9, 8.9]	0.641/0.4 [0.03–5.4]	0.668/0.8 [0.3–2.6]
SETD2 H-score (< 190 v ≥ 190)	0.261/1.7 [0.6, 5.2]	0.359/0.3 [0.02–4.3]	0.547/1.3 [0.4–3.8]

to the preexisting H3K4me3 mark suggesting that H3K4me3 is likely a downstream mark of H3K9 methylation. Additionally, the MLL2 SET domain was shown to methylate H3K4 in the presence of H3K9 methylation. In our study, the expression of MLL2 was higher in diffusely infiltrating astrocytomas, compared to pilocytic astrocytomas, denoting a differential pathogenetic implication of this histone modification between the two tumor types. Of importance, univariate survival analysis revealed a prognostic effect of MLL2 expression in the entire cohort with high MLL2 levels portending reduced patients' survival probability.

Another positive correlation was obtained between H3K9me3 levels and the active mark H3K36me3, suggesting a potential cooperative effect in gene regulation and possibly in the control of bivalent genes involved in cell cycle regulation and metabolism [43]. In our study, H3K36me3 immunoreactivity was observed in all cases, without any statistical difference between normal and neoplastic brain tissues. However, within diffusely infiltrating astrocytomas, high-grade cases displayed higher scores than grade II. Paradoxically, H3K36me3 expression levels were similar in pilocytic and high-grade diffuse astrocytomas. This is in accordance with the study of Pathak et al. that showed global H3K36 trimethylation in pediatric GBM. The cerebral hemisphere-specific G34R mutation has been shown to block H3K36 trimethylation by SETD2, impairing its catalytic activity [35]. In our cohort, we detected only two cases that harbored this mutation, which also exhibited low H3K36me3 expression. Furthermore, SETD2 levels were significantly increased in both pilocytic and diffusely infiltrating astrocytomas compared to normal brain tissues, indicating the implication of this methyltransferase in the early stages of the development of both groups of pediatric astrocytomas.

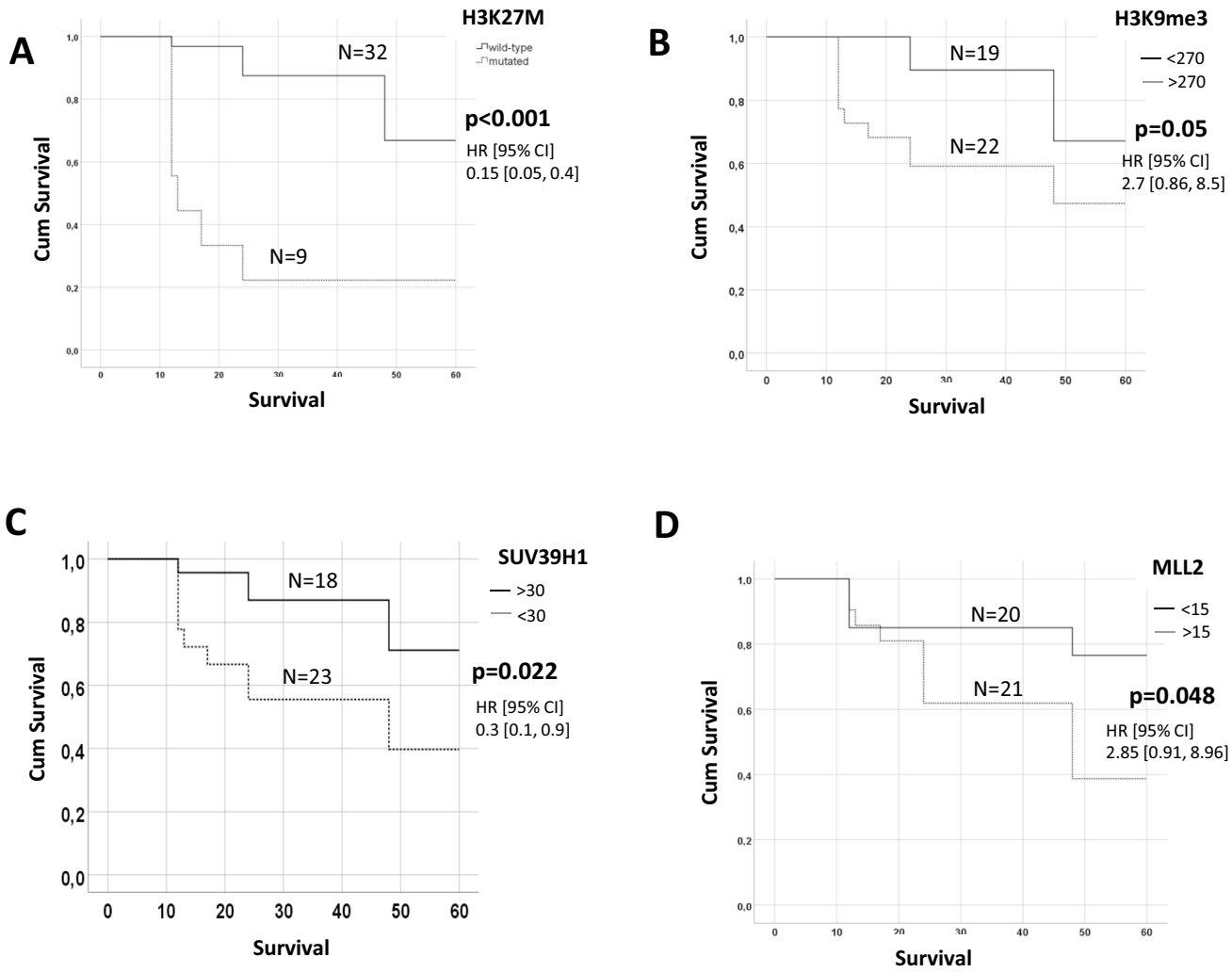

Fig. 6 Kaplan–Meier survival curves of H3K27M, H3K9me3, SUV39H1, and MLL2 in the entire cohort. **A** The presence of H3K27M mutant protein was associated with reduced survival. **B** Increased H3K9me3, **C** reduced SUV39H1, and **D** increased MLL2 expressions were associated with reduced survival in the entire cohort

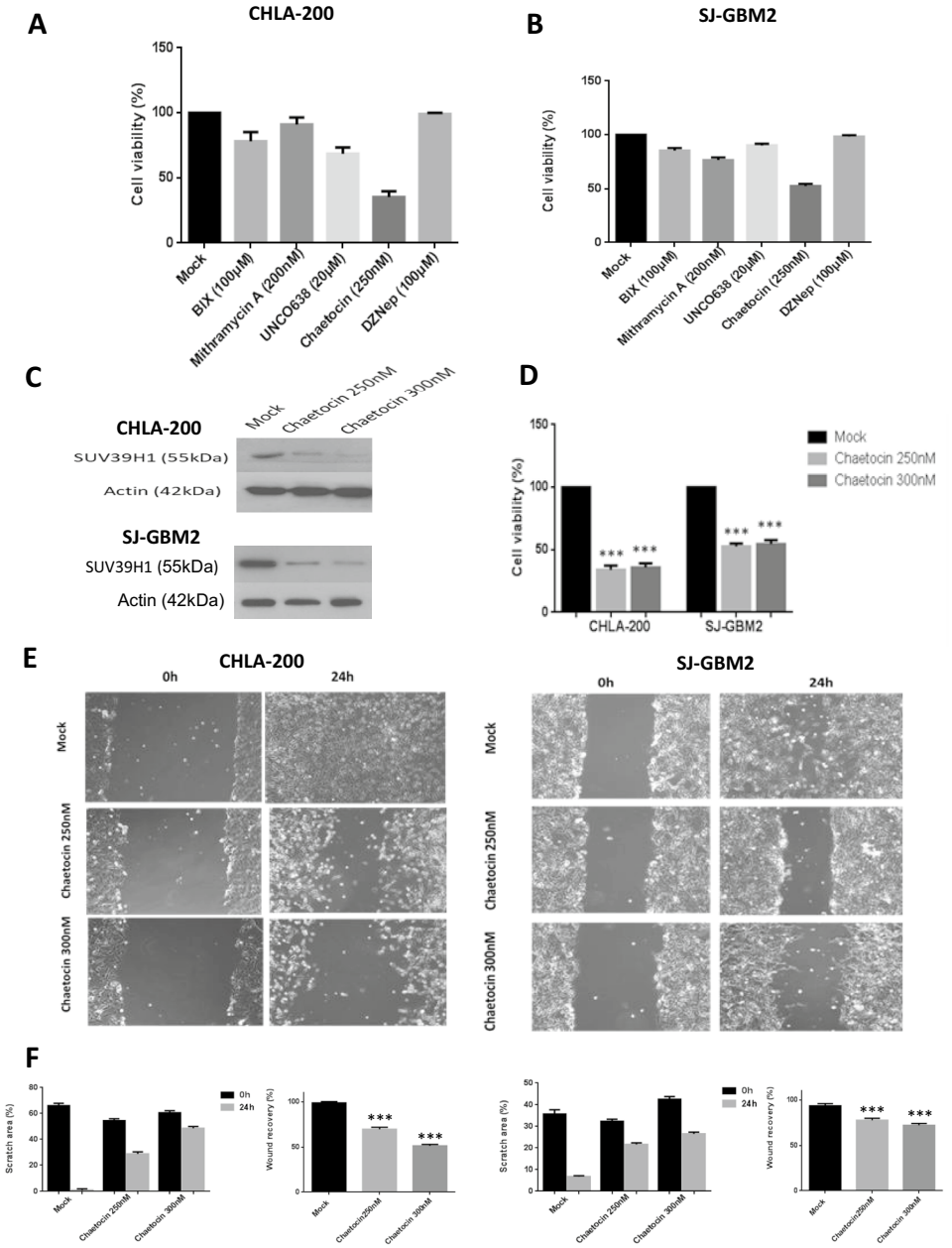

Fig. 7 **A**, **B** Treatment of pediatric astrocytoma cells CHLA-200 and SJ-GBM2 with selective histone and DNA methylation inhibitors. **C** Western blot analysis of SUV39H1 expression levels in both cell lines before and after chaetocin treatment. **D** XTT viability assays were performed in CHLA-200 and SJ-GBM2 cells at 48 h following treatment with chaetocin, indicating reduced cell proliferation compared to untreated cells ($p < 0.001$). **E** Monolayer scratch migration assay of CHLA-200 and SJ-GBM2 cells after chaetocin treatment. **F** Cell migration in the scratch area was calculated for chaetocin-treated CHLA-200 and SJ-GBM2 cells. Wound recovery was also estimated for chaetocin-treated cells compared to untreated controls ($p < 0.001$). All experiments were repeated at least three times, and representative data are shown (***$p < 0.001$)

Of interest, upregulation of H3K9me3-modifying enzymes, SETDB1 and SUV39H1 was observed in astrocytomas. SETDB1 expression was significantly increased in astrocytomas compared to normal brain tissues, increasing in parallel with the grade of diffusely infiltrating astrocytomas, thus indicating its important role in pediatric gliomagenesis. SETDB1 expression was positively correlated with H3K9me3 suggesting that this histone mark is preferentially established by SETDB1 in high-grade astrocytomas rather than by SUV39H1 methyltransferase. A similar pattern of SETDB1 levels was also previously reported for adult gliomas [13] and glioma cell lines [12]. Additionally, SETDB1 ablation in developing mouse brain has been shown to cause a decrease in H3K9 trimethylation [44].

The SUV39H1 methyltransferase on the other hand was increased in pilocytic astrocytomas, as compared to normal brain or diffusely infiltrating tumors, depicting a further difference in the pathogenetic mechanism underlying these two groups of pediatric astrocytic tumors. These findings imply that SUV39H1 plays a distinct role from SETDB1 in the regulation of chromatin remodeling in pediatric astrocytomas. It is likely that SUV39H1 establishes H3K9me3 in grade I tumors while SETDB1 establishes the same mark in high-grade cases as previously demonstrated in adult astroglial tumors [12, 13].

In favor of the emerging contribution of SUV39H1 in pediatric astrocytomas is the adverse prognostic effect of diminished expression levels that was revealed in the univariate analysis of the entire cohort and was maintained in multivariate analysis. In agreement with this finding, diminished nuclear SUV39H1 expression has been previously observed in adult glioblastomas and adversely affected patients' survival [13]. Bioinformatic analysis on the Cancer Genome Atlas (TCGA) and on a microarray dataset of 200 GBM samples, investigating the correlations between SUV39H1 and the 4 distinct GBM subtype signatures in pediatric glioblastomas, detected a positive correlation of SUV39H1 with proneural signature genes and a negative correlation with mesenchymal genes (data not shown). Since the proneural signature is associated with a better prognosis, whereas the mesenchymal one correlates with a poor clinical outcome, it may explain the association of diminished SUV39H1 expression with adverse patient survival observed in our study.

Further investigation of the functional significance of H3 methylation in astrocytomas with histone and DNA methylation inhibitors revealed that the SUV39H1 inhibitor, chaetocin, significantly reduced cell proliferation and migration of pediatric astrocytoma cell lines expressing high SUV39H1 levels, strengthening the functional implication of SUV39H1 in glioma progression. Future studies in pilocytic and diffusely infiltrating astrocytomas need to be conducted in larger cohorts to confirm its prognostic significance and biomarker potential.

Taken altogether, our data provide evidence on the deregulation of histone code in pediatric astrocytomas with predominant roles of H3K9me3, SUV39H1, and MLL2 in patients' prognosis, suggesting new molecular targets for therapy. The correlation of SUV39H1 methyltransferase with patients' survival and the validation of its functional role in the astrocytic tumor cells highlight its implication in their pathobiology and warrant verification in prospective investigations. Some limitations of the study include the small sample size, the lack of a more extensive genetic profiling including the KIAA1549-BRAF gene fusion and SETD2 and MLL2 mutations to enrich and better characterize the tissues. Also, the heterogeneity of treatments among patients as well as monitoring schedules may have had an impact on survival.

Overall, this primary study indicates a combination and potential cross talk of active and inactive histone marks, regulating cancer progression in pediatric astrocytomas. Follow-up experiments will be focused on the elucidation of molecular mechanisms characterizing different grades of astrocytomas. A series of ChIP-Seq experiments will be performed in normal brain and astrocytoma tissues, using antibodies against SUV39H1, SETDB1, and MLL2 and their respective histone marks (H3K9me3 and H3K4me3). In this way, we will explore the epigenetic landscape of the brain tumors and identify target genes that are differentially regulated and expressed in different grades by combining and integrating RNA-seq data. This approach will help us to uncover potential pathways and biomarkers in cancer progression.

The ultimate goal of our future studies will be to identify precision epiOmics maps that will enable us to stratify cancer patients. These studies will open a window towards precision and targeted medicine by including specific epigenetic inhibitors to current chemotherapy treatments.

Supplementary Information The online version contains supplementary material available at https://doi.org/10.1007/s13311-021-01090-x.

Acknowledgements We would like to thank Professor Anastasia Konstantinidou from the First Department of Pathology, Medical School, National and Kapodistrian University of Athens, for providing the archival normal brain tissues.

Required Author Forms Disclosure forms provided by the authors are available with the online version of this article.

Author Contribution PK, CP, AGP: conceptualization. AK, ANG, AM, MST, SS: methodology, investigation, software. AK, HK, MG, PK, CP: data curation, writing—original draft preparation. KAP, TK, GS: visualization, investigation. CP, AGP, PK: supervision. ANG, DSK, PK: software, validation. SC, CP, PK, AGP: writing—reviewing and editing.

Data Availability The data that support the findings of this study are openly available in Affymetrix Human Genome U133 Plus 2.0 Array—Platform GPL570) pediatric brain samples (GSE50161) at http://r2.amc.nl, reference number [36].

Declarations

Ethics Approval The research has been given ethical approval by the University of Athens Medical School Ethics Committee (27/06/2017, 1617031069).

Conflict of Interest The authors declare no competing interests.

References

1. Izycka-Swieszewska E, Bien E, Stefanowicz J, et al. Malignant gliomas as second neoplasms in pediatric cancer survivors: Neuropathological study. Biomed Res Int 2018:4596812. https://doi.org/10.1155/2018/4596812
2. Louis DN, Perry A, Reifenberger G, et al. The 2016 World Health Organization Classification of Tumors of the Central Nervous System: a summary. Acta Neuropathol 2016; 131: 803–820 https://doi.org/10.1007/s00401-016-1545-1.
3. Collins VP, Jones DTW, Giannini C. Pilocytic astrocytoma: pathology, molecular mechanisms and markers. Acta Neuropathol 2015; 129: 775–788 https://doi.org/10.1007/s00401-015-1410-7

4. Klonou A, Spiliotakopoulou D, Themistocleous MS, Piperi C, Papavassiliou AG. Chromatin remodeling defects in pediatric brain tumors. Ann Transl Med 2018; 6: 248–248. https://doi.org/10.21037/atm.2018.04.08
5. Gonçalves FG, Alves CAPF, Vossough A. Updates in pediatric malignant gliomas. Top Magn Reson Imaging 2020; 29: 83–94 https://doi.org/10.1097/RMR.0000000000000235.
6. Zhao Z, Shilatifard A. Epigenetic modifications of histones in cancer. Genome Biol 2019; 20:245. https://doi.org/10.1186/s13059-019-1870-5
7. Miller JL, Grant PA. The role of DNA methylation and histone modifications in transcriptional regulation in humans. Subcell Biochem 2013; 61: 289–317. https://doi.org/10.1007/978-94-007-4525-4_13
8. Bapat SA, Jin V, Berry N, et al. Multivalent epigenetic marks confer microenvironment-responsive epigenetic plasticity to ovarian cancer cells. Epigenetics 2010; 5: 717–730. https://doi.org/10.4161/epi.5.8.13014
9. Schotta G, Lachner M, Sarma K, et al. A silencing pathway to induce H3-K9 and H4-K20 trimethylation at constitutive heterochromatin. Genes Dev 2004; 18: 1251–1262. https://doi.org/10.1101/gad.300704
10. Becker JS, Nicetto D, Zaret KS. H3K9me3-Dependent Heterochromatin: Barrier to Cell Fate Changes. Trends Genet 2016; 32: 29–41 https://doi.org/10.1016/j.tig.2015.11.001
11. Zhou M, Li Y, Lin S, et al. H3K9me3, H3K36me3 , and H4K20me3 Expression Correlates with Patient Outcome in Esophageal Squamous Cell Carcinoma as Epigenetic Markers. Dig Dis Sci 2019; 64: 2147–2157. https://doi.org/10.1007/s10620-019-05529-2
12. Spyropoulou A, Gargalionis A, Dalagiorgou G, et al. Role of histone lysine methyltransferases SUV39H1 and SETDB1 in gliomagenesis: Modulation of cell proliferation, migration, and colony formation. NeuroMolecular Med 2014; 16: 70–82. https://doi.org/10.1007/s12017-013-8254-x
13. Sepsa A, Levidou G, Gargalionis A, et al. Emerging role of linker histone variant H1x as a biomarker with prognostic value in astrocytic gliomas. A multivariate analysis including trimethylation of H3K9 and H4K20. PLoS One 2015; 10: e0115101. https://doi.org/10.1371/journal.pone.0115101
14. Loyola A, Tagami H, Bonaldi T, et al. The HP1α-CAF1-SetDB1-containing complex provides H3K9me1 for Suv39-mediated K9me3 in pericentric heterochromatin. EMBO Rep 2009; 10: 769–775. https://doi.org/10.1038/embor.2009.90
15. Kleer CG, Cao Q, Varambally S, et al. EZH2 is a marker of aggressive breast cancer and promotes neoplastic transformation of breast epithelial cells. Proc Natl Acad Sci USA 2003; 100: 11606–11611. https://doi.org/10.1073/pnas.1933744100
16. Chen YN, Hou SQ, Jiang R, Sun JL, Cheng CD, Qian ZR. EZH2 is a potential prognostic predictor of glioma. J Cell Mol Med 2020; 25: 925–936. https://doi.org/10.1111/jcmm.16149
17. Bracken AP, Pasini D, Capra M, Prosperini E, Colli E, Helin K. EZH2 is downstream of the pRB-E2F pathway, essential for proliferation and amplified in cancer. EMBO J 2003; 22: 5323–5335. https://doi.org/10.1093/emboj/cdg542
18. Bernstein BE, Humphrey EL, Erlich RL, et al. Methylation of histone H3 Lys 4 in coding regions of active genes. Proc Natl Acad Sci USA 2002; 99: 8695–8700. https://doi.org/10.1073/pnas.082249499
19. Chen K, Chen Z, Wu D, et al. Broad H3K4me3 is associated with increased transcription elongation and enhancer activity at tumor-suppressor genes. Nat Genet 2015; 47: 1149–1157. https://doi.org/10.1038/ng.3385
20. Bogeas A, Morvan-Dubois G, El-Habr EA, Lejeune FX, Defrance M, Narayanan A, Kuranda K, Burel-Vandenbos F, Sayd S, Delaunay V, Dubois LG, Parrinello H, Rialle S, Fabrega S, Idbaih A, Haiech J, Bièche I, Virolle T, Goodhardt M, Chneiweiss H, Junier MP. Changes in chromatin state reveal ARNT2 at a node of a tumorigenic transcription factor signature driving glioblastoma cell aggressiveness. Acta Neuropathol. 2018; 135(2): 267-283. https://doi.org/10.1007/s00401-017-1783-x.
21. Ellinger J, Kahl P, Mertens C, et al. Prognostic relevance of global histone H3 lysine 4 (H3K4) methylation in renal cell carcinoma. Int J Cancer 2010; 127: 2360–2366. https://doi.org/10.1002/ijc.25250
22. Wen H, Li Y, Xi Y, et al. ZMYND11 links histone H3.3K36me3 to transcription elongation and tumour suppression. Nature 2014; 508: 263–268. https://doi.org/10.1038/nature13045
23. Li M, Cheng J, Ma Y, et al. The histone demethylase JMJD2A promotes glioma cell growth via targeting Akt-mTOR signaling. Cancer Cell Int 2020; 20:101. https://doi.org/10.1186/s12935-020-01177-z
24. Viaene AN, Santi M, Rosenbaum J, Li MM, Surrey LF, Nasrallah MP. SETD2 mutations in primary central nervous system tumors. Acta Neuropathol Commun 2018; 6: 123. https://doi.org/10.1186/s40478-018-0623-0
25. Zaravinos A, Bizakis J, Spandidos DA. RKIP and BRAF aberrations in human nasal polyps and the adjacent turbinate mucosae. Cancer Lett 2008; 264: 288–298. https://doi.org/10.1016/j.canlet.2008.01.046
26. Theodoropoulos G, Papaconstantinou I, Felekouras E, et al. Relation between common polymorphisms in genes related to inflammatory response and colarectal cancer. World J Gastroenterol 2006; 12: 5037–5043. https://doi.org/10.3748/wjg.v12.i31.5037
27. Griesinger AM, Birks DK, Donson AM, et al. Characterization of Distinct Immunophenotypes across Pediatric Brain Tumor Types. J Immunol 2013; 191: 4880–4888. https://doi.org/10.4049/jimmunol.1301966
28. Klaus B, Reisenauer S. An end to end workflow for differential gene expression using Affymetrix microarrays [version 2]. F1000Research 2018; 5:1384. https://doi.org/10.12688/f1000research.8967.2
29. Vandel J, Gheeraert C, Staels B, Eeckhoute J, Lefebvre P, Dubois-Chevalier J. GIANT: galaxy-based tool for interactive analysis of transcriptomic data. Sci Rep 2020; 10:19835. https://doi.org/10.1038/s41598-020-76769-w
30. Huber W, Carey VJ, Gentleman R, et al. Orchestrating high-throughput genomic analysis with Bioconductor. Nat Methods 2015; 12: 115–121. https://doi.org/10.1038/nmeth.3252
31. Koster J, Volckmann R, Zwijnenburg D, Molenaar P, Versteeg R. R2: Genomics analysis and visualization platform Cancer Res 2019; 79:2490. Abstract.
32. Huang T, Garcia R, Qi J, Lulla R, Horbinski C. Detection of histone H3 K27M mutation and post-translational modifications in pediatric diffuse midline glioma via tissue immunohistochemistry informs diagnosis and clinical outcomes. Oncotarget 2018; 9: 37112–37124 https://doi.org/10.18632/oncotarget.26430
33. Chan KM, Fang D, Gan H, et al. The histone H3.3K27M mutation in pediatric glioma reprograms H3K27 methylation and gene expression. Genes Dev 2013; 27: 985–990. https://doi.org/10.1101/gad.217778.113
34. Lee CH, Yu JR, Granat J, Saldaña-Meyer R, et al. Automethylation of PRC2 promotes H3K27 methylation and is impaired in H3K27M pediatric glioma. Genes Dev 2019; 33: 1428–1440. https://doi.org/10.1101/gad.328773.119
35. Pathak P, Jha P, Purkait S, et al. Altered global histone-trimethylation code and H3F3A-ATRX mutation in pediatric GBM. J Neurooncol 2015; 121: 489–497. https://doi.org/10.1007/s11060-014-1675-z
36. Bender S, Tang Y, Lindroth AM, et al. Reduced H3K27me3 and DNA hypomethylation are major drivers of gene expression in K27M mutant pediatric high-grade gliomas. Cancer Cell 2013; 24: 660–672. https://doi.org/10.1016/j.ccr.2013.10.006
37. Mohammad, F, Weissmann, S, Leblanc, B, et al. EZH2 is a potential therapeutic target for H3K27M-mutant pediatric gliomas. Nat Med 2017; 23, 483–492. https://doi.org/10.1038/nm.4293.
38. Ahsan S, Raabe EH, Haffner MC, et al. Increased 5-hydroxymethylcytosine and decreased 5-methylcytosine are indicators of

global epigenetic dysregulation in diffuse intrinsic pontine glioma. Acta Neuropathol Commun 2014; 2: 59. https://doi.org/10.1186/2051-5960-2-59
39. Venneti S, Felicella MM, Coyne T, et al. Histone 3 lysine 9 trimethylation is differentially associated with isocitrate dehydrogenase mutations in oligodendrogliomas and high-grade astrocytomas. J Neuropathol Exp Neurol 2013; 72: 298–306. https://doi.org/10.1097/NEN.0b013e3182898113
40. Yoshimoto K, Hatae R, Sangatsuda Y, Suzuki SO. Prevalence and clinicopathological features of H3.3 G34-mutant high-grade gliomas : a retrospective study of 411 consecutive glioma cases in a single institution. Brain Tumor Pathol 2017; 34: 103–112. https://doi.org/10.1007/s10014-017-0287-7
41. Deng H, Zeng J, Zhang T, et al. Histone H3.3K27M mobilizes multiple cancer/testis (CT) antigens in pediatric glioma. Mol Cancer Res 2018; 16: 623–633. https://doi.org/10.1158/1541-7786.MCR-17-0460
42. Matsumura Y, Nakaki R, Inagaki T, et al. H3K4/H3K9me3 Bivalent Chromatin Domains Targeted by Lineage-Specific DNA Methylation Pauses Adipocyte Differentiation. Mol Cell 2015; 60: 584–596. https://doi.org/10.1016/j.molcel.2015.10.025
43. Mauser R, Kungulovski G, Keup C, Reinhardt R, Jeltsch A. Application of dual reading domains as novel reagents in chromatin biology reveals a new H3K9me3 and H3K36me2/3 bivalent chromatin state. Epigenetics and Chromatin 2017; 10: 45. https://doi.org/10.1186/s13072-017-0153-1
44. Tan S-L, Nishi M, Ohtsuka T, et al. Essential roles of the histone methyltransferase ESET in the epigenetic control of neural progenitor cells during development. Development 2012; 139: 3806– 3816. https://doi.org/10.1242/dev.082198

Authors and Affiliations

Alexia Klonou[1] · Penelope Korkolopoulou[2] · Antonios N. Gargalionis[1] · Dimitrios S. Kanakoglou[2] · Hector Katifelis[3] · Maria Gazouli[3] · Sarantis Chlamydas[1] · Andreas Mitsios[4] · Theodosis Kalamatianos[5] · George Stranjalis[5] · Marios S. Themistocleous[4] · Kostas A. Papavassiliou[1] · Spyros Sgouros[6] · Athanasios G. Papavassiliou[1] · Christina Piperi[1]

1 Department of Biological Chemistry, Medical School, National and Kapodistrian University of Athens, 75 Mikras Asias Street, 11527 Athens, Greece

2 First Department of Pathology, Medical School, National and Kapodistrian University of Athens, 11527 Athens, Greece

3 Laboratory of Biology, Medical School, National and Kapodistrian University of Athens, 11527 Athens, Greece

4 Department of Neurosurgery, Agia Sofia' Children's Hospital, Medical School, National and Kapodistrian University of Athens, 11527 Athens, Greece

5 Department of Neurosurgery, 'Evangelismos' Hospital, Medical School, National and Kapodistrian University of Athens, 10676 Athens, Greece

6 Department of Pediatric Neurosurgery, 'Mitera' Children's Hospital, Medical School, National and Kapodistrian University of Athens, 15123 Athens, Greece